Linear instability of a zigzag pattern

Tommy Dessup, Thibaud Maimbourg, Christophe Coste, and Michel Saint Jean

Laboratoire "Matière et Systèmes Complexes" (MSC), UMR 7057 CNRS, Université Paris 7 Diderot, 75205 Paris Cedex 13, France

Interacting particles confined in a quasi-one-dimensional channel are physical systems which display various equilibrium patterns according to the interparticle interaction and the transverse confinement potential. Depending on the confinement, the particles may be distributed along a straight line, in a staggered row (zigzag), or in a configuration in which the linear and zigzag phases coexist (distorted zigzag). In order to clarify the conditions of existence of each configuration, we have studied the linear stability of the zigzag pattern. We find an acoustic transverse mode that destabilizes the zigzag configuration for short-range interaction potentials, and we calculate the interaction range above which this instability disappears. In particular, we recover the unconditional stability of zigzag patterns for Coulomb interactions. We show that the domain of existence for the distorted zigzag patterns is accurately described by our linear stability analysis. We also emphasize the complexity of finite size effects. Last, we provide a criterion for the onset of instability in the thermodynamic limit and propose a biphasic model that explains some characteristics of the distorted zigzag patterns.

I. INTRODUCTION

Many physical systems are constituted by interacting particles confined in narrow channels, moving in a way that keeps the particles' order, for instance, molecules moving through cell membrane channels [1], laser-cooled ions confined in Paul traps [2–5], optically confined paramagnetic colloidal particles [6], plasma dusts in electrostatic traps [6–9], and electrostatically interacting macroscopic beads [10–12]. These confined systems give rise to interesting questions about their stable equilibrium configurations. Indeed, according to the interparticle interaction range, to the particle density or to the size of the narrow channel, the particles arrange either along a straight line or in a staggered row, called hereafter a zigzag, or in heterogeneous configurations where zigzag and linear patterns coexist. For instance ions confined electromagnetically in Paul traps [2–5] always exhibit homogeneous configurations, either aligned or zigzag depending on the confinement. On the other hand, in plasma dust experiments [6–9,13] or for electrostatically interacting beads in macroscopic systems [12,14–16], heterogeneous configurations are also observed. The main goal of this paper is to clarify the origin of this diversity.

These systems may be modeled to a first approximation as interacting point particles transversally confined in a quasi-one-dimensional (1D) cell by a quadratic potential. Two relevant energies compete to produce their equilibrium configurations: the repulsive interparticle interaction characterized by its amplitude and its range, and the transverse potential which confines the particles and keeps their order. When the confinement is much stronger than the interaction potential, the particles are always distributed along a straight line corresponding to the minimum of the confinement potential. When the confinement is lowered, becoming comparable to the interparticle interaction, a staggered zigzag row may become energetically favorable, since the energy lost by climbing the transverse potential up is counterbalanced by the decrease of interaction energy due to the greater interparticle distance in the zigzag pattern. However, the coexistence of linear and zigzag phases in equilibrium configurations observed in some experiments suggests a modulationnal instability of the zigzag

pattern, such that the stable equilibrium actually is a distorted zigzag pattern.

Each kind of stable configuration results from specific conditions, which we identify by looking at the linear stability of the zigzag configuration. We derive the vibrational eigenmodes for a generic interparticle interaction in Sec. II. In Sec. III we show that one mode may become unstable, with a purely imaginary eigenfrequency. We identify the relevant parameters and exhibit the essential role of the interaction range. In particular, we justify the stability of the zigzag pattern for Coulomb interactions [4,17–19], whereas it may be unstable for dipolar interactions [20,21] or for other finite range interactions [7–9]. In this last case, we determine a stability criterion depending upon the particle density and the confinement stiffness, which accounts for the diversity of observed configurations. Finally, in Sec. IV we confront our predictions with equilibrium configurations obtained by molecular dynamics simulations.

II. VIBRATIONAL EIGENMODES OF THE ZIGZAG CONFIGURATION

Let us consider a zigzag configuration of length L for $2N$ identical point particles of mass m ($m = 2.15$ mg in the simulations) held in the plane xOy. In the longitudinal direction (x direction) we assume periodic boundary conditions. In the transverse direction (y direction) the particles are confined by an harmonic potential of stiffness β. Each of the N unit cells of this periodic configuration contains two particles $\{A_p^0, B_p^0\}$ (see Fig. 1) of respective coordinates $\{2pd, -h\}$ and $\{(2p+1)d, +h\}$ where d is the longitudinal interparticle distance $L/(2N)$ and where h is the "zigzag height" defined as the transverse distance between the particle and the bottom line of the confinement potential (considered as the x axis in the following). In what follows, d is kept constant, such that $d = 1.875$ mm; that is, $N = 16$ unit cells is a system of length $L = 60$ mm. These peculiar values of the parameters are chosen to be consistent with experimental works [8–11].

These particles interact with a repulsive potential of energy scale U_0 and of characteristic range λ_0. In order to allow a direct
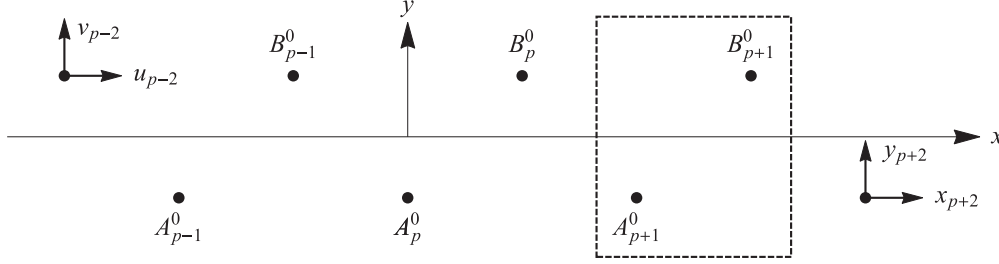
FIG. 1. A zigzag configuration, showing a unit cell (dashed box). We also show the small displacements of the particles at equilibrium positions A_{p+2}^0 and B_{p-2}^0.

comparison between other experiments or simulations and our results, we will apply potentials such as the three-dimensional (3D) Coulomb interaction, the 3D dipolar interaction, the Yukawa potential, and the modified Bessel function $K_0(\cdot)$ interaction (relevant for superconductor vortices and experiments with macroscopic beads) [10,11]. For Yukawa and modified Bessel potentials, the finiteness of the interaction range allows us to write this potential as $U(r) \equiv U_0 f(r/\lambda_0)$. To allow the comparison between the potentials, we choose the energy scale in such a way that the nearest neighbors' interaction energy is the same with all potentials. For $d/\lambda_0 = 3.91$, we take $U_0 f(d/\lambda_0)/k_B = 8.5 \times 10^{12}$ K, where k_B is Boltzmann constant.

In order to deal with all interaction potentials within the same formalism, we take into account all possible interparticle interactions. For short-range interaction it would be sufficient to consider only a finite number of neighbors: for instance, we have shown that in the case of a typical modified Bessel interaction, keeping only the two closest neighbors is enough to obtain the eigenfrequencies with a good precision [11,12].

With periodic boundary conditions, the potential energy is the same for each particle in the staggered row, so that the energy of the system reads

$$E = 2N \left[\sum_{j=1}^{N} U\left(\sqrt{d_j^2 + 4h^2}\right) + \sum_{j=1}^{N-1} U(2jd) + \frac{\beta}{2} h^2 \right],$$
(1)

where $d_j \equiv (2j-1)d$. The resulting mechanical equilibrium equation shows that a zigzag configuration with $h \neq 0$ exists only below a critical confinement value $\beta_{ZZ} = 4 \sum_{j=1}^{N} F(d_j)/d_j$ where $F(r) = -U'(r)$. For a strong confinement, $\beta \geqslant \beta_{ZZ}$, all the particles stand on a straight line ($h = 0$) corresponding to the transverse potential minimum [12,15,22],

while for a confinement $\beta < \beta_{ZZ}$ and a given interparticle distance d, the zigzag height h is implicitly given as a function of β by

$$\beta = 4 \sum_{j=1}^{N} \frac{F\left(\sqrt{d_j^2 + 4h^2}\right)}{\sqrt{d_j^2 + 4h^2}}.$$
(2)

For the modified Bessel potential and $d/\lambda_0 = 3.91$, we have $\beta_{ZZ} = 5.82 \times 10^{-4}$ N/m, which corresponds to an energy $\beta_{ZZ} d^2/k_B = 1.5 \times 10^{14}$ K and to a frequency $\sqrt{\beta_{ZZ}/m} = 16.5$ s^{-1}.

To analyze the linear stability of the zigzag equilibrium, we compute its vibrational eigenmodes in the linear approximation. The coordinates of the particles are $A_p = \{2pd + x_p(t), -h + y_p(t)\}$ and $B_p = \{(2p+1)d + u_p(t), + h + v_p(t)\}$ where $|x_p|$, $|y_p|$, $|u_p|$ and $|v_p|$ are much smaller displacements than either d or h (see Fig. 1).

The potential energy of the system is

$$E = \sum_{p=1}^{N} \left\{ \sum_{j=1}^{N} [U(A_p B_{p+j-1}) + U(B_p A_{p+j})] \right.$$
$$\left. + \sum_{j=1}^{N-1} [U(A_p A_{p+j}) + U(B_p B_{p+j})] \right\}$$
$$+ \frac{\beta}{2} \sum_{p=1}^{N} [(y_p - h)^2 + (v_p + h)^2],$$
(3)

where the periodic boundary condition imply that indices which are congruent modulo N correspond to the same particle. Expanding this energy up to second order with respect to the small displacements, and using the Euler-Lagrange equation, we find the linearized equations of motion:

$$m\ddot{x}_p = \sum_{j=1}^{N} [K_{xx}(j)(u_{p-j} + u_{p+j-1} - 2x_p) + K_{xy}(j)(v_{p-j} - v_{p+j-1})] + \sum_{j=1}^{N-1} K(2jd)(x_{p+j} + x_{p-j} - 2x_p),$$
(4)

$$m\ddot{y}_p = \sum_{j=1}^{N} [K_{yy}(j)(v_{p-j} + v_{p+j-1} - 2y_p) + K_{xy}(j)(u_{p-j} - u_{p+j-1})] + \sum_{j=1}^{N-1} \frac{F(2jd)}{2jd}(y_{p+j} + y_{p-j} - 2y_p) - \beta y_p,$$
(5)

$$m\ddot{u}_p = \sum_{j=1}^{N} [K_{xx}(j)(x_{p+j} + x_{p-j+1} - 2u_p) + K_{xy}(j)(y_{p+j} - y_{p-j+1})] + \sum_{j=1}^{N-1} K(2jd)(u_{p+j} + u_{p-j} - 2u_p),$$
(6)

$$m\ddot{v}_p = \sum_{j=1}^{N}[K_{yy}(j)(y_{p+j} + y_{p-j+1} - 2v_p) + K_{xy}(j)(x_{p+j} - x_{p-j+1})] + \sum_{j=1}^{N-1}\frac{F(2jd)}{2jd}(v_{p+j} + v_{p-j} - 2v_p) - \beta v_p, \quad (7)$$

where

$$K_{xx}(j) = \frac{(2j-1)^2 d^2}{r_j^2}K(r_j) - \frac{4h^2}{r_j^3}F(r_j), \tag{8}$$

$$K_{yy}(j) = \frac{4h^2}{r_j^2}K(r_j) - \frac{(2j-1)^2 d^2}{r_j^3}F(r_j), \tag{9}$$

$$K_{xy}(j) = \frac{2(2j-1)dh}{r_j^2}\left[K(r_j) + \frac{F(r_j)}{r_j}\right], \tag{10}$$

$$r_j \equiv \sqrt{(2j-1)^2 d^2 + 4h^2}, \quad F(r_j) = -\left.\frac{\partial U}{\partial r}\right|_{r_j}, \quad K(r_j) = \left.\frac{\partial^2 U}{\partial r^2}\right|_{r_j}. \tag{11}$$

Here the coefficients $K_{lm}(j)$ correspond to the stiffness arising from the interactions between particles separated by a distance r_j, when the displacements are in the direction l ($l = x$ or y) for the first particle and in the direction m for the second one. Notice that K_{xy} is proportional to the zigzag height h.

Owing to the periodic boundary conditions, the vibrational displacements may be expanded in Fourier modes. For instance, $x_{p+N} = x_p$ and

$$\tilde{x}(s,t) = \frac{1}{N}\sum_{j=1}^{N}x_j(t)e^{-i\frac{2\pi}{N}sj} \quad \text{and} \quad x_j(t) = \sum_{s=1}^{N}\tilde{x}(s,t)e^{i\frac{2\pi}{N}sj}. \tag{12}$$

From the Eq. (4)–(7) we obtain the dynamic matrix $\mathbb{M}(h)$, whose eigenvalues are the vibrational frequencies of the system:

$$\mathbb{M}(h) \equiv \begin{pmatrix} -2C_{xx}(s) & 2e^{-i\phi(s)}C_{xu}(s) & 0 & 2ie^{-i\phi(s)}C_{xv}(s) \\ 2e^{i\phi(s)}C_{xu}(s) & -2C_{xx}(s) & -2e^{i\phi(s)}C_{xv}(s) & 0 \\ 0 & 2ie^{-i\phi(s)} - C_{xv}(s) & \beta - 2C_{yy}(s) & 2e^{-i\phi(s)}C_{yv}(s) \\ -2ie^{i\phi(s)}C_{xv}(s) & 0 & 2e^{i\phi(s)}C_{yv}(s) & \beta - 2C_{yy}(s) \end{pmatrix}, \tag{13}$$

where $\phi(s) = \pi s/N$ is the dimensionless wave number, and where

$$C_{xx}(s) = \sum_{j=1}^{N}K_{xx}(j) + 2\sum_{j=1}^{N-1}K(2jd)\sin^2[j\phi(s)], \quad C_{xu}(s) = \sum_{j=1}^{N}K_{xx}(j)\cos[(2j-1)\phi(s)],$$

$$C_{xv}(s) = \sum_{j=1}^{N}K_{xy}(j)\sin[(2j-1)\phi(s)], \tag{14}$$

$$C_{yy}(s) = \sum_{j=1}^{N}K_{yy}(j) + \sum_{j=1}^{N-1}\frac{F(2jd)}{jd}\sin^2[j\phi(s)], \quad C_{yv}(s) = \sum_{j=1}^{N}K_{yy}(j)\cos[(2j-1)\phi(s)]. \tag{15}$$

When $h = 0$ (for $\beta \geqslant \beta_{ZZ}$), all the coefficients $K_{xy}(j)$ vanish so that $C_{xv}(s) = 0$ and the dynamic matrix $\mathbb{M}(h = 0)$ is block-diagonal:

$$\mathbb{M}(h = 0) \equiv \begin{pmatrix} -2C_{xx}(s) & 2e^{-i\phi(s)}C_{xu}(s) & 0 & 0 \\ 2e^{i\phi(s)}C_{xu}(s) & -2C_{xx}(s) & 0 & 0 \\ 0 & 0 & \beta - 2C_{yy}(s) & 2e^{-i\phi(s)}C_{yv}(s) \\ 0 & 0 & 2e^{i\phi(s)}C_{yv}(s) & \beta - 2C_{yy}(s) \end{pmatrix}. \tag{16}$$

This block structure reflects the fact that the longitudinal vibrations (left upper block) are independent from the transverse vibrations (right lower block) for linear chains as it was previously shown [11,12].

Four vibrational branches, with eigenmodes indexed by the wave vector $\phi(s) = 2\pi s/(2N)$ with $-N/2 \leqslant s \leqslant N/2$ are obtained (the modes at the edges $\pm N/2$, corresponding to the same displacements, have by convention a weight 1/2, so that there are exactly N modes). Hereafter, in order to get the eigenmodes at the Brillouin zone edges, we assume that the cell number N is even. The squared eigenfrequencies $\omega^2(s)$ of $\mathbb{M}(h = 0)$, corresponding to the linear chain,

are given by

$$m\left(\omega_{AL}^0\right)^2 = 2[C_{xu}(s) - C_{xx}(s)], \quad \text{(longitudinal acoustic)}$$

$$m\left(\omega_{OL}^0\right)^2 = -2[C_{xx}(s) + C_{xu}(s)], \quad \text{(longitudinal optical)}$$

$$m\left(\omega_{AT}^0\right)^2 = \beta - 2C_{yy}(s) - 2C_{yv}(s), \quad \text{(transverse acoustic)}$$

$$m\left(\omega_{OT}^0\right)^2 = \beta - 2C_{yy}(s) + 2C_{yv}(s), \quad \text{(transverse optical)}$$

$$(17)$$

with the corresponding eigenvectors $[\mathbf{V}_{AL}^0, \mathbf{V}_{OL}^0, \mathbf{V}_{AT}^0, \mathbf{V}_{OT}^0]$. They have been calculated previously in Refs. [11] and [12] and are valid for $\beta \geqslant \beta_{ZZ}$.

These squared frequencies are plotted in Fig. 2(a) for $\beta > \beta_{ZZ}$ and in Fig. 2(b) for $\beta = \beta_{ZZ}$. Notice that for convenience we have described the system with a model of two particles per cell even if the equilibrium configuration is linear. So these curves display the usual shape of phonon dispersions in a crystal with two atoms per cell. The Brillouin zone folding induces degeneracies for $\phi(s = N/2)$ of the acoustic and optical branches for longitudinal and transverse polarizations. In each case the longitudinal acoustic branch exhibits a zero frequency mode for $s = 0$ and displays a parabolic dependency $\omega^2 \propto s^2$ at small s. This mode results from the longitudinal translation invariance of the linear chain. Exactly at the zigzag

transition, $\beta = \beta_{ZZ}$, a second mode of zero frequency appears in the transverse acoustic branch [see Fig. 2(b)]. This mode, which appears only at the zigzag transition, is the soft mode at the transition which would be observed at $\phi = \pm\pi$ in the unfolded first Brillouin zone [15].

Another point to keep in mind is that the transverse acoustic branch corresponds to an unusual relative displacement of particles. While the acoustic displacements are ordinary in phase, here the transverse acoustic displacements in the same cell are in opposite phase. Indeed, this reflects the balance between the energy increase due to the confinement potential and the interaction energy decrease due to a larger distance between the particles.

When $\beta < \beta_{ZZ}$, $h \neq 0$ and K_{xy} takes a finite value. It is convenient to write the full dynamical coupling matrix $\mathbb{M}(h)$ on the basis of the eigenvectors obtained for $h = 0$. This dynamic matrix is given by $\hat{\mathbb{M}}(h) = \mathbb{B}_0^{-1} \cdot \mathbb{M}(h) \cdot \mathbb{B}_0$ where $\mathbb{B}_0$ is the square matrix built with the column eigenvectors $[\mathbf{V}_{OL}^0, \mathbf{V}_{OT}^0, \mathbf{V}_{AL}^0, \mathbf{V}_{AT}^0]$ written on the basis of the displacements (x, u, y, v):

$$\mathbb{B}_0 = \frac{1}{\sqrt{2}} \begin{pmatrix} -e^{-i\phi(s)} & 0 & e^{-i\phi(s)} & 0 \\ 1 & 0 & 1 & 0 \\ 0 & e^{i\phi(s)} & 0 & -e^{-i\phi(s)} \\ 0 & 1 & 0 & 1 \end{pmatrix}. \quad (18)$$

On this basis, $\hat{\mathbb{M}}(h)$ also has a block diagonal structure:

$$\begin{pmatrix} -2(C_{xu} + C_{xx}) & -2iC_{xv} & 0 & 0 \\ 2iC_{xv} & 2\left(C_{yv} - C_{yy} + \frac{\beta}{2}\right) & 0 & 0 \\ 0 & 0 & 2(C_{xu} - C_{xx}) & 2iC_{xv} \\ 0 & 0 & -2iC_{xv} & 2\left(-C_{yy} - C_{yv} + \frac{\beta}{2}\right) \end{pmatrix}. \quad (19)$$

The upper left block matrix connects the two optical eigenmodes obtained for $h = 0$. So, for convenience, the corresponding eigenmodes will be improperly named hereafter "optical modes," even if they are not. Similarly the bottom right block matrix involves the "acoustic modes." Their eigenvalues are given by

$$m\omega_{OL}^2 = T_{O-} + \sqrt{4C_{xv}^2 + T_{O+}^2},$$

$$m\omega_{OT}^2 = T_{O-} - \sqrt{4C_{xv}^2 + T_{O+}^2}, \quad (20)$$

$$m\omega_{AL}^2 = T_{A-} + \sqrt{4C_{xv}^2 + T_{A+}^2},$$

$$m\omega_{AT}^2 = T_{A-} - \sqrt{4C_{xv}^2 + T_{A+}^2} \quad (21)$$

with

$$T_{O\pm}(s) = \frac{\beta}{2} - C_{yy}(s) + C_{yv}(s) \pm [C_{xx}(s) + C_{xu}(s)], \quad (22)$$

$$T_{A\pm}(s) = \frac{\beta}{2} - C_{yy}(s) - C_{yv}(s) \pm [C_{xx}(s) - C_{xu}(s)]. \quad (23)$$

The evolution of the dispersion equations (20) and (21) for $\beta < \beta_{ZZ}$, hence $h \neq 0$, are displayed in Figs. 2(c) and 2(d). We

recover the four expected branches but their shapes are strongly modified with respect to those obtained for $h = 0$. In particular, the degeneracy at $\phi(0) = 0$ of the two "acoustic modes," observed for $\beta = \beta_{ZZ}$, now disappears. This effect traces back to the fact that $C_{xy} \neq 0$. Thus only the "transverse acoustic mode" remains a genuine acoustic mode with a parabolic dependency $\omega^2 \propto s^2$ at small s [see Figs. 2(c) and 2(d)]. This mode is linked to the translational invariance, which is a symmetry of the zigzag pattern, as it is of the linear chain. As seen in Eqs. (20) and (21) the coupling between acoustic (respectively optical) modes induces repulsion of the corresponding branches. This anticrossing can be large enough to move the squared acoustic transverse frequency towards negative values for $s > 0$, resulting in the appearance of unstable modes in the zigzag configuration. This is shown in the inset of Fig. 2(c) and in Figs. 3(b) and 3(c).

III. BEHAVIOR OF THE TRANSVERSE ACOUSTIC MODE

In this section we will focus on the transverse acoustic mode [denoting its eigenfrequency $\omega^2(\phi) \equiv \omega_{AT}^2(\phi)$] and explore the conditions under which its squared frequency takes a negative value, which means the onset of an instability of the zigzag pattern. We shall look at the influence of the interaction
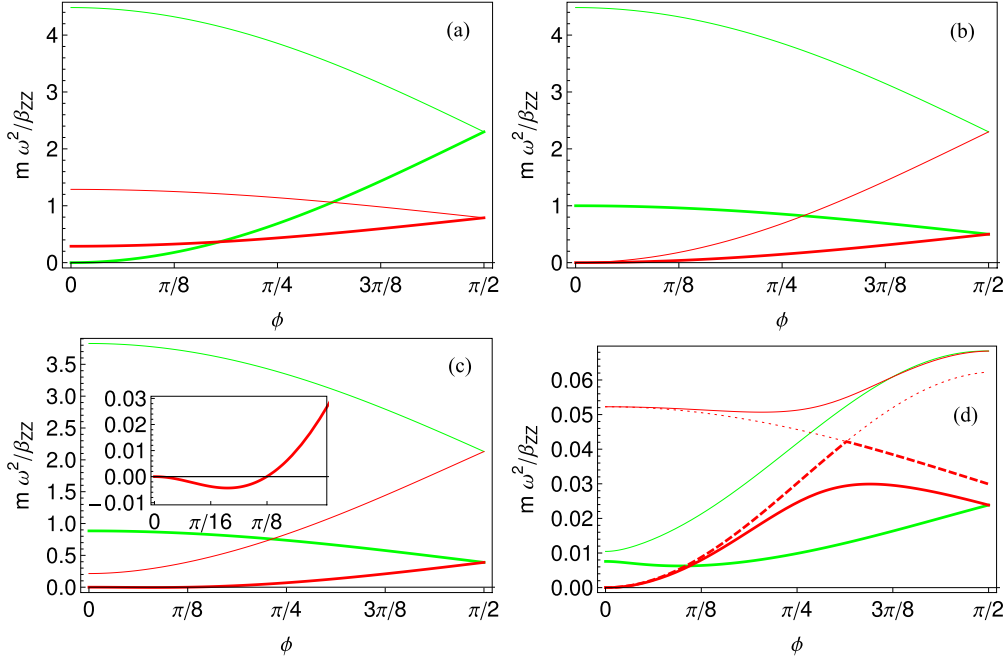
FIG. 2. (Color online) Dimensionless squared frequencies $m\omega^2/\beta_{ZZ}$ of the acoustic transverse [thick red (dark gray) line] and longitudinal [thick green (light gray) line] mode and of the optical transverse [red (dark gray) line] and longitudinal [green (light gray) line] modes as a function of the dimensionless wave number ϕ for an infinite system. The interaction potential is the modified Bessel function, with $d/\lambda_0 = 3.91$; hence $\beta_{ZZ} = 5.82 \times 10^{-4}$ N/m. (a) $\beta = 10^{-3}$ N/m (straight line, $h = 0$); (b) just at the threshold $\beta = \beta_{ZZ}$; (c) $\beta = 5.15 \times 10^{-4}$ N/m [thus a zigzag pattern of height $h = 0.2$ mm; see Eq. (2)], and the inset is a zoom on the acoustic transverse mode plot; (d) $\beta = 4.41 \times 10^{-6}$ N/m [thus a zigzag pattern of height $h = 1.6$ mm; see Eq. (2)]. The dashed and dotted plots show the squared frequencies when the off-diagonal terms in the matrix (19) are not taken into account.

potential and more specifically the role of its range on the instability of the zigzag pattern.

Let us consider an infinite system of interacting particles in a zigzag pattern characterized by d and h. The variations of ω^2 with $\phi(s)$ calculated for a 3D Coulomb interparticle potential is presented in Fig. 3(a) for two values of h. These squared frequencies are always positive in agreement with Ref. [17].

Very different behaviors are observed for short-range potentials, such as the modified Bessel and Yukawa potentials. The corresponding dispersion curves calculated for two different h are shown in Figs. 3(b) and 3(c), respectively. In these cases, the squared value ω^2 may be negative for particular values of h/d and ϕ.

In actual systems, finite size effects have to be included. For a system of $2N$ particles, the smallest (nonzero) value of ϕ is π/N. As an example, we display in Fig. 4 the squared eigenfrequencies for 32, 64, and 128 particles. All discrete values are distributed along the generic curve obtained for an infinite system. All squared eigenfrequencies are positive for 32 particles, whereas those corresponding to the smallest wave vectors are negative for larger systems (64 or 128 particles) (see Fig. 4). Thus, for the same interparticle distance and the same transverse stiffness, a zigzag pattern that is unstable for an infinite system may be stable for a sufficiently small finite system.

In order to proceed further in the instability analysis, it is convenient to plot the contour line $\omega^2 = 0$ in the plane
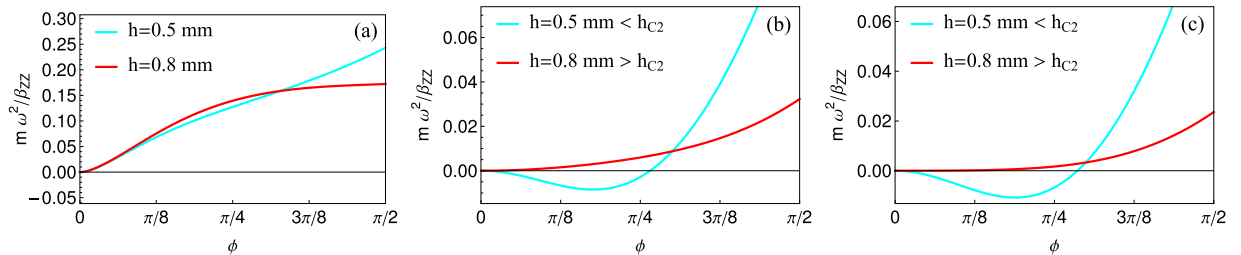

FIG. 3. (Color online) Dimensionless squared frequencies $m\omega^2/\beta_{ZZ}$ of the transverse acoustic mode as a function of the dimensionless wave number ϕ for an infinite system. Interaction potentials are (a) 3D Coulomb ($\beta_{ZZ} = 1.40 \times 10^{-4}$ N/m, $\beta = 9.80 \times 10^{-5}$ N/m for $h = 0.5$ mm, and $\beta = 6.48 \times 10^{-5}$ N/m for $h = 0.8$ mm); (b) modified Bessel function ($\beta_{ZZ} = 5.82 \times 10^{-4}$ N/m, $\beta = 2.84 \times 10^{-4}$ N/m for $h = 0.5$ mm, and $\beta = 1.11 \times 10^{-4}$ N/m for $h = 0.8$ mm); (c) Yukawa ($\beta_{ZZ} = 6.52 \times 10^{-4}$ N/m, $\beta = 2.94 \times 10^{-4}$ N/m for $h = 0.5$ mm, and $\beta = 1.05 \times 10^{-4}$ N/m for $h = 0.8$ mm). For cases (b) and (c) the interaction range is $d/\lambda_0 = 3.91$. The energy scales are such that the nearest neighbors interactions for $h = 0$ are the same for all three potentials. The critical threshold h_{C2} is defined in Eq. (29).
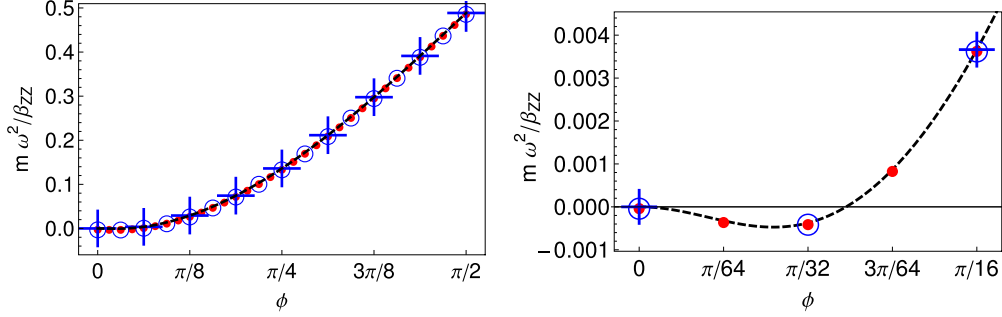
FIG. 4. (Color online) Illustration of finite size effects. The black dashed line is the plot of the dimensionless squared frequency $m\omega^2/\beta_{ZZ}$ as a function of the dimensionless wave number ϕ for an infinite system, with modified Bessel interaction potential, $d/\lambda_0 = 3.91$ and $h = 0.06$ mm ($\beta = 5.76 \times 10^{-4}$ N/m). Discrete modes are shown for 32 particles (blue crosses), 64 particles (blue circles), and 128 particles (red dots). The right plot is a zoom at small wave number.

$(h/d, \phi)$ for several short-range potentials, as done in Fig. 5. In the closed domain defined by the h/d axis and the contour line, we have $\omega^2(h/d, \phi) \leqslant 0$. An infinite system is thus unstable inside this domain (hereafter named "instability domain") and stable outside. We plot in Fig. 5(a) the instability domain for a modified Bessel interaction and several interaction ranges for a constant energy scale U_0. We see that the area of the instability domain decreases when the interaction range increases. The same behavior is observed with the Yukawa potential, as shown in Fig. 5(b). Concerning the 3D dipolar interaction, which is a finite range potential with a much larger range than modified Bessel or Yukawa potential, the instability domain is of much smaller size [see Fig. 5(c)]. Consistently, there is no instability domain in the case of 3D Coulomb interaction (see Appendix A), which is the limit of the Yukawa potential for $\lambda_0 \to \infty$. In contrast, in the limit of a very short range which allows the restriction to nearest neighbor interactions, the zigzag pattern displays a long wavelength ($\phi \ll 1$) instability for all h [see the black solid line in Figs. 5(a) and 5(b) and Eq. (25)].

The influence of the interaction potential characteristics on the zigzag stability may be more precisely quantified. For small ϕ, the dispersion equation (21) may be written

$-m\omega^2 = S(h)\phi^2$ where $S(h)$ is given by

$$S(h) = \sum_{j=1}^{N-1} (2j)^2 K(2jd) + \sum_{j=1}^{N} (2j-1)^2 K_{xx}(j)$$
$$+ \frac{\left[\sum_{j=1}^{N} (2j-1) K_{xy}(j)\right]^2}{\left|\sum_{j=1}^{N} \left[K_{yy}(j) - \frac{F(r_j)}{r_j}\right]\right|}. \tag{24}$$

The instability of the zigzag pattern corresponds to a positive $S(h)$ since the curvature of the dispersion relation at the origin is then negative. When the interactions are limited to the nearest neighbors, a straightforward calculation gives

$$S(h) = \frac{F(r_1)}{4r_1}, \tag{25}$$

which is positive for repulsive interactions, whatever the zigzag amplitude h. If only nearest neighbors interactions are included, any zigzag pattern in an infinite system is unstable towards long wavelength ($\phi \to 0$) perturbations. This is shown by the black dashed lines in Figs. 5(a) and 5(b). Next nearest neighbor interactions, at least, are necessary to stabilize the zigzag pattern and forbid its collapse.
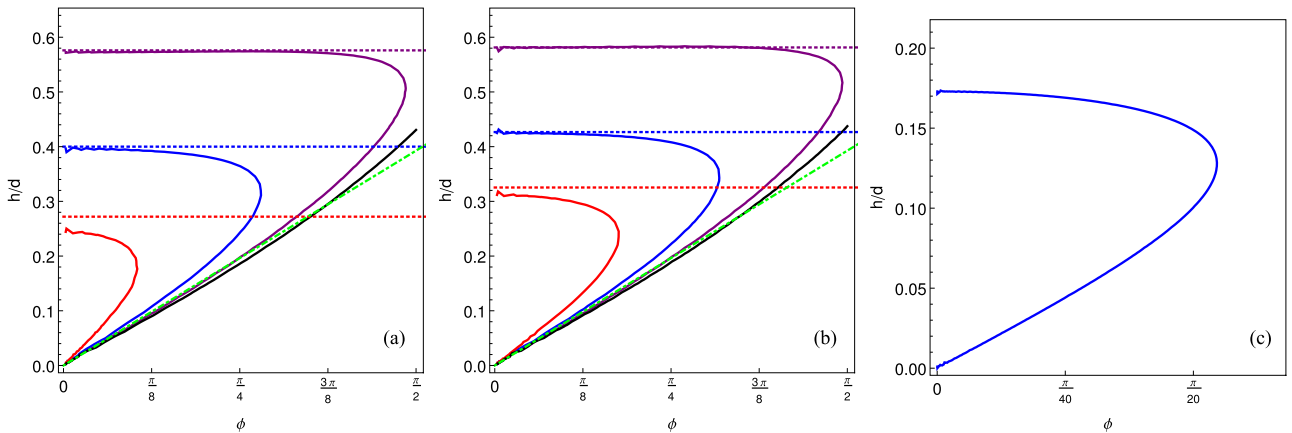

FIG. 5. (Color online) Contour line $\omega^2(h/d, \phi) = 0$ in the plane $(h/d, \phi)$. The interaction potential is (a) modified Bessel; (b) Yukawa; (c) 3D dipolar interactions (notice the scale on both axes). For panels (a) and (b) the colors indicate the interaction range, $d/\lambda_0 = 7.81$ (purple, outer curve), 3.91 (blue, intermediate curve), and 2.60 (red, inner curve). The black solid line is the contour line when only nearest neighbors interactions are taken into account [Eq. (25)]. The green (light gray) dashed lines correspond to the threshold h_{C1} (Eq. (28)) and the colored dotted lines to the threshold h_{C2} [Eq. (29)].
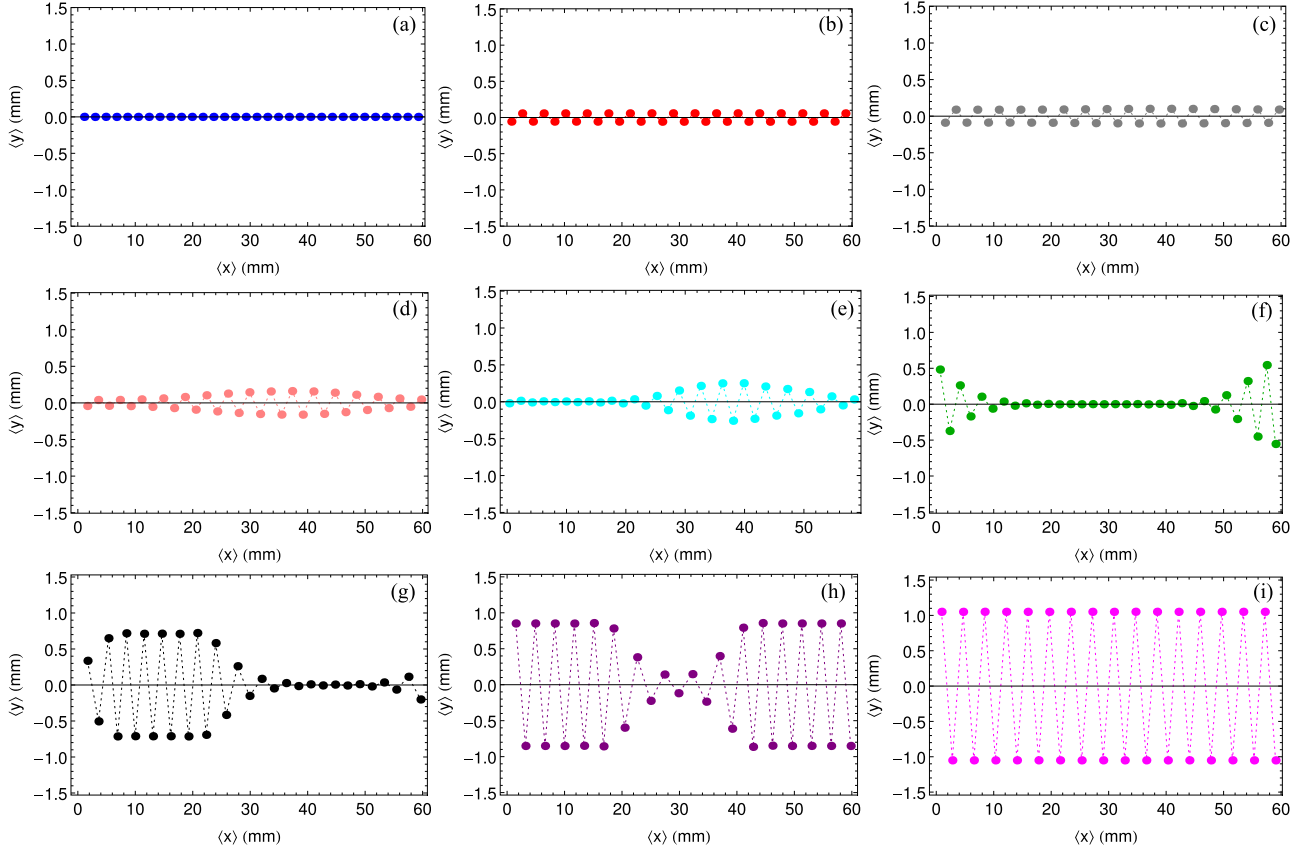
FIG. 6. (Color online) Equilibrium position $\langle y \rangle$ in function of $\langle x \rangle$ in mm for a periodic system of 32 particles, of length $L = 60$ mm and at $T = 10^9$ K. The interaction potential is the modified Bessel function, and $\beta_{ZZ} = 5.82 \times 10^{-4}$ N/m. The numerical values of β / β_{ZZ} are as follows: (a) 1.004; (b) 0.98; (c) 0.96; (d) 0.95; (e) 0.93; (f) 0.89; (g) 0.52; (h) 0.22; (i) 0.07.

An explicit expression of the marginal stability curve which encloses the instability domain is not available, but an approximation, valid at small h, may be obtained. It is done in Appendix A in the particular case of a power law interaction,

$$U_\alpha(r) = U_0 \frac{d^\alpha}{r^\alpha}, \tag{26}$$

where it is shown that the zigzag pattern is stable for $\alpha \leqslant \alpha_c = 2.645$. For 3D Coulomb interaction ($\alpha = 1$) an infinite system is always stable, whereas for dipolar interaction ($\alpha = 3$) an infinite system is unstable [Fig. 5(c)]. For modified Bessel and Yukawa interaction the system is unstable as soon as $d/\lambda_0 > 2.04$ and $d/\lambda_0 > 1.49$ respectively (see Appendix B). Notice that this is consistent with the stability for 3D Coulomb interaction for which $\lambda_0 \to \infty$. On the other hand, for very short-range interactions ($\lambda_0 \to 0$), the condition is broken and the system is unstable.

Let us consider now a zigzag pattern of amplitude h_0 in a finite system of $2N$ particles. For such systems the location of the point $(h_0/d, \pi/N)$ determines the stability of the zigzag pattern. If we assume that the interaction range is small enough for the point $(h_0/d, \phi = \pi/N)$ to be in the instability domain, the system is unstable for $h_{C1} < h_0 < h_{C2}$. We compute estimates of these two thresholds in order to obtain a semi-quantitative criterion of instability.

From Eqs. (21) and (23), we may simplify the definition of the marginal stability curve, $\omega_{AT}^2 = 0$, as

$$\left[\frac{\beta}{2} - C_{yy}(s) - C_{yv}(s) \right] [C_{xx}(s) - C_{xu}(s)] = C_{xv}(s)^2, \tag{27}$$

where β is given as a function of h using Eq. (2). To determine the lower threshold h_{C1} we benefit from the fact that at small h and ϕ, the curve $\omega^2(h,\phi) = 0$ calculated with first neighbors only is tangent to the curve that takes into account all the interactions [see Figs. 5(a) and 5(b)]. It is therefore sufficient to estimate h_{C1} in the nearest neighbors approximation. Expanding for small h Eq. (27), we obtain for the threshold h_{C1}

$$\frac{h_{C1}}{d} \approx \frac{\pi s}{4N} \sqrt{\frac{K(r_1)}{K(r_1) + F(r_1)/r_1}} \approx \frac{\pi s}{4N} = \frac{\phi}{2}, \tag{28}$$

since $F(r_1)/r_1$ is much smaller than $K(r_1)$.

In Figs. 5(a) and 5(c), we see that the other threshold h_{C2} is nearly independent of ϕ. Thus we expand Eq. (27) at small ϕ, taking into account second neighbors interactions because they are a necessary condition for h_{C2} to exist. We find that h_{C2} satisfies

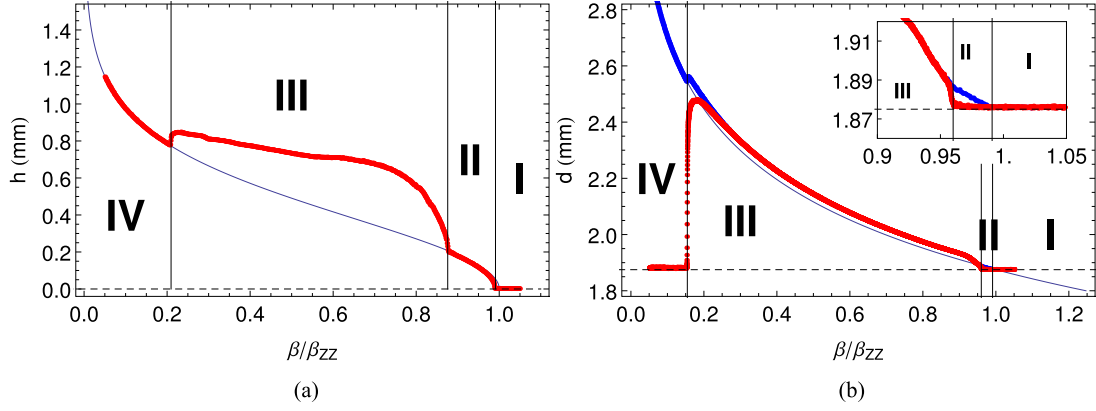$$\frac{F(\sqrt{d^2 + 4h_{C2}^2})}{\sqrt{d^2 + 4h_{C2}^2}} + 4K(2d) \approx 0. \tag{29}$$

FIG. 7. (Color online) (a) The thin solid blue line is the zigzag height h of a perfect zigzag pattern, as a function of the normalized confinement β/β_{ZZ} with $\beta_{ZZ} = 5.82 \times 10^{-4}$ N/m. The thick red dots represent the highest height h measured in the simulations for 16 particles. (b) The thin solid blue line corresponds to $l^*(\beta)$ in Eq. (30), the thick red (dark gray) and blue (light grey) dots are, respectively, the maximal longitudinal distance and the maximal AB distance as a function of the normalized confinement for 32 particles. For both plots the interaction is a modified Bessel potential, with $d/\lambda_0 = 3.91$.

Figure 5 shows the very good agreement between these estimates and the contour line $\omega^2(h/d, \phi) = 0$. The only discrepancy happens for h_{C2} at the largest values of the potential range. This is consistent since taking only next nearest neighbors interactions becomes a poor approximation at large interaction range.

IV. DISTORTED ZIGZAG PATTERNS INSIDE THE INSTABILITY DOMAIN

In this section, our analytical results are compared with molecular dynamics simulations, using a modified Bessel interaction potential. However, the details of the potential do not matter for the results presented in this section. The numerical algorithm has already been described elsewhere [11,12]. Basically, we simulate coupled Langevin equations with uncorrelated thermal noise on each particle, taking into account all interparticle interactions. We use periodic boundary conditions in the longitudinal (x) direction, and the particles are confined in the transverse (y) direction by an harmonic potential of stiffness β. We study the equilibrium configurations of a system with $2N$ particles, varying the transverse stiffness.

In Fig. 6 we display the equilibrium configurations obtained as β varies for a system of 32 particles confined in a channel of length $L = 60$ mm, decreasing the transverse stiffness from top to bottom and left to right. In this finite size system, the minimal nonzero wave number is $\pi/16$. For strong confinement values, $\beta > \beta_{ZZ}$, the particles are aligned on the x axis [Fig. 6(a)]. When β decreases under β_{ZZ}, while $h(\beta)$ is still below $h_{C1}(\pi/16)$, the stable configuration is a zigzag pattern [Figs. 6(b) and 6(c)]. When β reaches a critical value such that $h(\beta) = h_{C1}(\pi/16)$, the zigzag pattern becomes unstable. A spatially modulated zigzag configuration is seen in Fig. 6(d). Now the zigzag height is local and depends upon the particle positions along the x axis. When β is further decreased, part of the particles are staggered while the others stay aligned along the x axis. We call this localized zigzag pattern a *bubble*. When the β decrease is carried on, the main

effect is that more and more particles become involved in the bubble, which increases slowly in amplitude [Figs. 6(e)–6(h)]. When $h(\beta)$ reaches h_{C2}, all the particles are at the same height and a large amplitude zigzag pattern is recovered [Fig. 6(i)].

These patterns are summarized in Fig. 7(a), where we plot the maximum zigzag height h as a function of the dimensionless stiffness β/β_{ZZ}. Zone I corresponds to $\beta/\beta_{ZZ} > 1$, thus to aligned particles with $h = 0$ [Fig. 6(a)]. Zone II corresponds to the small amplitude zigzag pattern, $h < h_{C1}$ [Figs. 6(b) and 6(c)]. Zone III corresponds to the heterogeneous zigzag patterns, with $h_{C1} \leqslant h \leqslant h_{C2}$ [Figs. 6(d)–6(h)]. Zone IV corresponds to the large amplitude zigzag, $h > h_{C2}$ [Fig. 6(i)]. We compare in Fig. 7(a) the measured zigzag height with the expectation for a perfect zigzag, given by Eq. (2). The agreement is excellent when the equilibrium configuration is an homogeneous pattern (zones I, II, and IV). Notice in particular that the agreement is still very good even far from the threshold (zone IV). In contrast, in zone III where heterogeneous patterns are observed, the measured h is greater than for a perfect zigzag. It means an increase of confinement energy for the particles in the bubble, which is compensated by a decrease in interaction energy. When compared to a zigzag pattern, the particles inside the bubble are thus at a larger distance from their neighbors but, as we shall see, this is also true for the particles outside the bubble. Thus the interaction energy is decreased for every particle.

In Fig. 8 we plot the results of systematic measurements of h_{C1} and h_{C2}, which define zone III of Fig. 7(a). The mean interparticle distance d and the interaction potential are kept constant, and we vary the system size, taking $2N$ particles ($2N = 8, 16, 32, 64$) in a periodic cell of length $L = 2Nd$. The measurements of the critical zigzag heights h_{C1} and h_{C2} are compared to the solution of Eq. (27) for an infinite system. As shown by Fig. 8, the measured values are in perfect agreement with the threshold calculated in the thermodynamic limit.

In order to better understand the distorted zigzag patterns, a simple biphasic model can be proposed. In a system of an even number of identical particles with periodic boundary conditions, the longitudinal distance between nearest neighbors
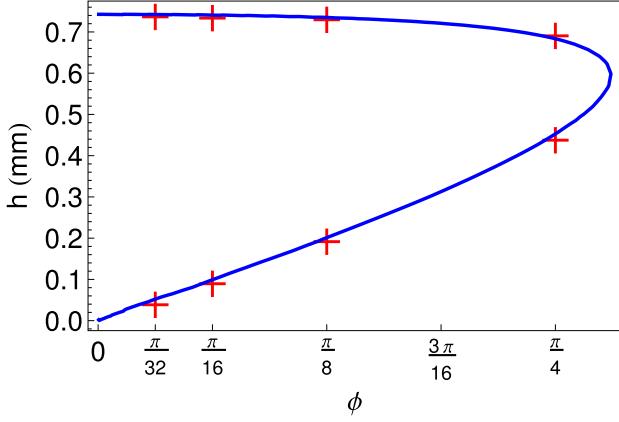
FIG. 8. (Color online) The blue curve is the marginal stability curve $\omega^2 = 0$, in the plane (ϕ, h), which is the blue curve in Fig. 5(a). The red crosses are the threshold h_{C1} and h_{C2} measured on simulations for several numbers of particles, $N = 32, 16, 8,$ and 4 from left to right.

is a constant, $d = L/(2N)$, whether they are aligned along the x axis or in a zigzag pattern. In this latter case, the first neighbor distances are also constant, equal to $\sqrt{d^2 + 4h^2}$. It is thus of interest to measure the first neighbor distance AB and its projection along the x axis for distorted zigzag patterns.

The variations of these distances with the particle rank are presented in Fig. 9 for the patterns displayed in Fig. 6. When the equilibrium pattern is heterogeneous, the longitudinal distance is greater for the particles that are aligned along the x axis than for the ones that are in the bubble. This effect is due to the geometric reduction of longitudinal force between adjacent particles in the bubble, which allow the particles outside the bubble to expand. Moreover, we notice that the AB distance is

roughly a constant, whether the particles are inside or outside the bubble. We will call l^* this constant distance between nearest neighbors. In Fig. 9 we see that l^* increases as the confinement decreases, while the number of particles inside the bubble increases.

This apparent adaptation of AB distance allows to interpret, in a first approximation, an heterogeneous zigzag pattern as the coexistence of a linear phase, in which all particles are aligned along the x axis, and a localized zigzag phase (the bubble). For this picture to be correct, both the linear phase and the zigzag phase must be at equilibrium under the applied transverse confinement. The transverse confinement has therefore to be exactly at its marginal stability value for a system of particles which are separated by l^*. Thus l^* must verify the following equation:

$$\beta = 4\frac{F(l^*)}{l^*}. \tag{30}$$

In Fig. 9 we compare the measured values of l^* with the solution $l^*(\beta)$ of Eq. (30) and see that the agreement is indeed excellent.

The AB and longitudinal distances are plotted versus the dimensionless stiffness β/β_{ZZ} in Fig. 7(b), for 32 particles. When the particles are aligned (zone I) or in a zigzag pattern (zones II and IV), the longitudinal distance is equal to the mean interparticle distance d. We see clearly that for heterogeneous zigzag patterns (zone III) the longitudinal distance outside the bubble and the AB distance inside the bubble are equal, and in very good agreement with the distance $l^*(\beta)$. This distance increases smoothly when the transverse confinement decreases, and nothing particular is seen when the modulated zigzag patterns are replaced by bubbles [compare, for example, Figs. 6(d) and 6(e)].

The linear stability theory of Sec. II explains the domain of existence of the heterogeneous patterns. The shape of the
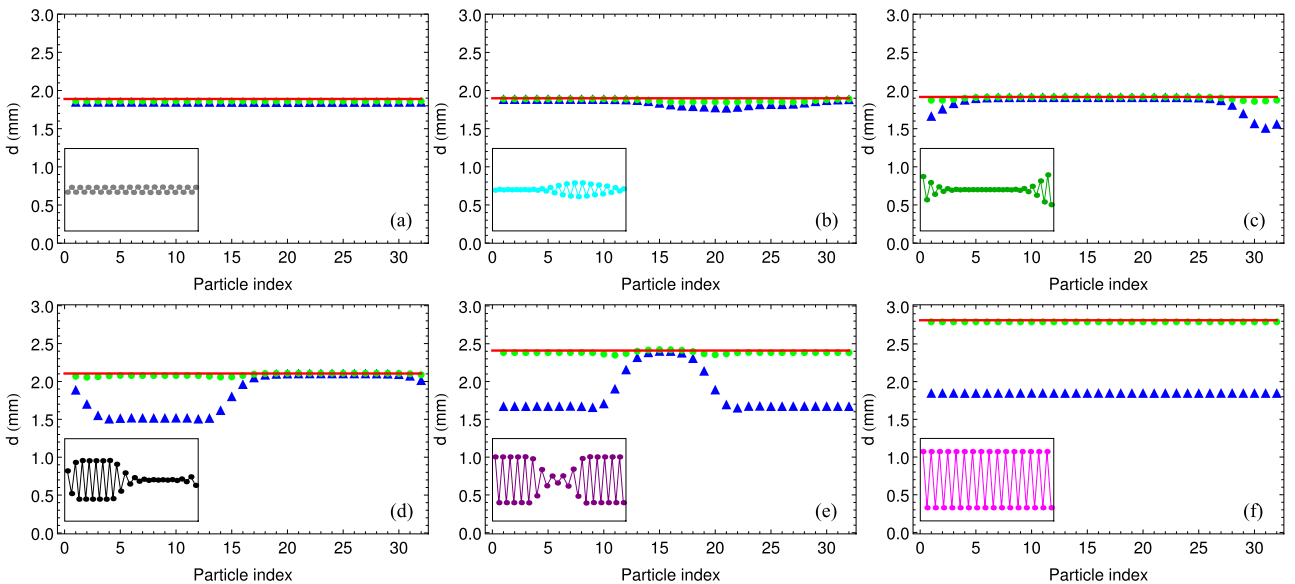

FIG. 9. (Color online) Plot of the distance d (mm) as a function of the particles index. For green (light gray) disks d is the AB distance between neighboring particles and for blue (dark gray) triangles d is their x distance, for the simulations of Fig. 6. In inset we display the corresponding pattern. The amplitude of the confinement potential, β, decreases from top to bottom and left to right, corresponding to $\beta/\beta_{ZZ} = 0.96, 0.95, 0.93, 0.89, 0.22,$ and 0.07. The solid red line shows the distance $l^*(\beta)$ defined in Eq. (30).
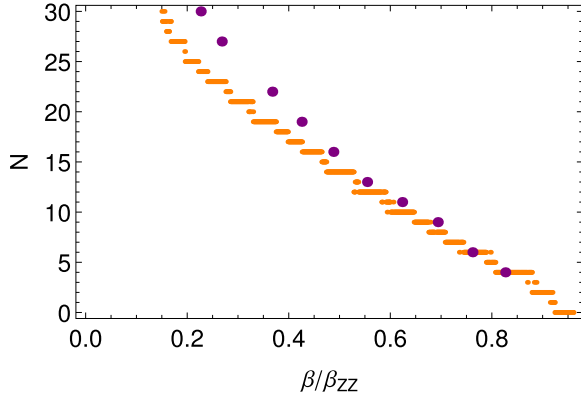
FIG. 10. (Color online) In orange (light gray), plot of the number of particles N in a bubble as a function of the dimensionless transverse stiffness β/β_{ZZ}, for a simulation with 32 particles in a canal of length $L = 60\,\text{mm}$. The purple (dark gray) dots correspond to the estimated N_{ZZ} obtained by the minimization of the energy in Eq. (31).

bubbles depends on the nonlinear interactions between the particles and cannot be described in the linear approximation. They are the subject of a forthcoming paper [16]. Nevertheless, the existence of a single interparticle distance l^* in heterogeneous patterns gives some insight into the bubbles shape. Indeed, we may roughly describe a bubble with N_L and N_{ZZ} particles, respectively, in a linear or zigzag configuration, requiring $N_L + N_{ZZ} = 2N$ (which amounts to neglect the particles involved in the edges of the bubble, where h depends on the position). The energy associated to a given bubble is then estimated taking into account the interactions between first and second neighbors, since nearest neighbors interactions do not forbid bubble collapse. It reads

$$E_{\text{bubble}} \sim N_L[U(l^*) + U(2l^*)] + N_{ZZ}[U(l^*) + U(2d_{ZZ})]$$
$$+ N_{ZZ}\frac{\beta(l^{*2} - d_{ZZ}^2)}{8}, \tag{31}$$

where d_{ZZ} is the longitudinal distance between the particles in the zigzag bubble, in such a way that the bubble height is $(l^{*2} - d_{ZZ}^2)/4$. In our simple model, the distance d_{ZZ} is such that

$$N_{ZZ}d_{ZZ} = L - (N_L - N_{ZZ})l^*. \tag{32}$$

The minimization of E_{bubble}, taking into account this constraint, and at constant β hence at constant l^*, gives an estimate of N_{ZZ}. In Fig. 10 we compare this estimate to the number of particles that take part in the bubble, as a function of the

transverse stiffness β. Despite the crudeness of our analysis, the comparison exhibits a very good agreement. The small discrepancy may be attributed to the fact that our simple model does not carefully account for the bubble edges.

V. SUMMARY

Systems of interacting particles confined by a transverse potential display a large variety of configurations, according to the relative influence of the transverse confinement, to the interaction potential, characterized by its range and amplitude, and to the number of particles. At equilibrium, the particles may be organized in a straight line, in a staggered row (zigzag configuration) or in heterogeneous pattern that we call bubbles, in which a straight line and a staggered row coexist. This variety is due to the instability of the zigzag configuration, characterized by the existence of a pure imaginary eigenfrequency in its transverse acoustic vibration branch.

In infinite systems, the study of this transverse acoustic mode shows that zigzag patterns in Coulomb systems are always stable. On the other hand, for finite range interactions the zigzag pattern may be unstable. This is evidenced by an instability domain in the plane $(h/d, \phi)$ where h is the zigzag height and ϕ the wave number. For a given interparticle distance, the area of this instability domain increases when the interaction range decreases.

For finite systems, the situation is slightly more complex. The discreteness of the vibrational modes implies that the smallest nonzero mode may be outside the instability domain, for sufficiently small number of particles, whatever the zigzag height h. In such small systems, the zigzag is thus stable. If the system size is large enough, we observe when the transverse confinement decreases a small zigzag, then a heterogeneous pattern and eventually a large stable zigzag. The relevant zigzag amplitude thresholds for the instability of the zigzag pattern has been determined as a function of N and λ_0 in Eqs. (28) and (29).

Gradually releasing the confinement, the unstable pattern evolves from a zigzag to a modulated structure, then to an heterogeneous bubble where some particles exhibit a zigzag pattern, and are surrounded by particles that are in a straight line. The heterogeneous pattern is characterized by the distance between nearest neighbors, which is constant in the whole system, and corresponds to the interparticle distance for which an infinite system would be marginally stable for the same confinement. A more quantitative analysis of these nonlinear patterns will be developed in a forthcoming paper [16].

APPENDIX A: INSTABILITY CRITERION AT SMALL h

In this Appendix, we calculate the small h expansion of $S(h)$, defined in Eq. (24). Because of the symmetry $h \leftrightarrow -h$, this expansion reads

$$S(h) = S_0 + S_2 h^2 + O(h^4). \tag{A1}$$

An instability happens when $S(h) \geq 0$. The instability at small h is observed if there is a real root $\sqrt{-S_0/S_2}$.
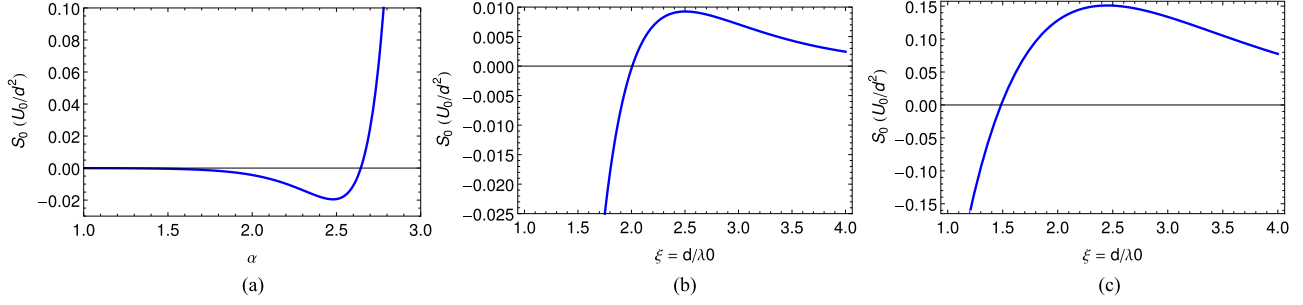
FIG. 11. (Color online) (a) Plot of S_0 as a function of α for power law potentials; (b) and (c) plots of S_0 as a function of ξ for modified Bessel and Yukawa interactions, respectively. In all plots we use the natural unit U_0/d^2 for S_0.

A tedious, but straightforward calculation shows that

$$S_0 = \sum_{j=1}^{N}[(2j)^2 K(2jd) + (2j-1)^2 K(d_j)] + \frac{\left\{ \sum_{j=1}^{N} \left[K(d_j) - \frac{F(d_j)}{d_j} \right] \right\}^2}{\left| \sum_{j=1}^{N} \left[\frac{K(d_j)}{d_j^2} - \frac{F(d_j)}{d_j^3} \right] \right|} \tag{A2}$$

and

$$S_2 = 4 \sum_{j=1}^{N} (2j-1)^2 \left[\frac{F(d_j)}{d_j^3} + \frac{K'(d_j)}{2d_j} - \frac{K(d_j)}{d_j^2} \right] + 4 \frac{\sum_{j=1}^{N} \left[K(d_j) - \frac{F(d_j)}{d_j} \right]}{\left| \sum_{j=1}^{N} \left[\frac{K(d_j)}{d_j^2} - \frac{F(d_j)}{d_j^3} \right] \right|} \sum_{j=1}^{N} \left[\frac{3F(d_j)}{d_j^3} + \frac{K'(d_j)}{d_j} - \frac{3K(d_j)}{d_j^2} \right]$$

$$+ \frac{\sum_{j=1}^{N} \left[\frac{6F(d_j)}{d_j^5} + \frac{2K'(d_j)}{d_j^3} - \frac{6K(d_j)}{d_j^4} \right] \left\{ \sum_{j=1}^{N} \left[K(d_j) - \frac{F(d_j)}{d_j} \right] \right\}^2}{\left\{ \sum_{j=1}^{N} \left[\frac{K(d_j)}{d_j^2} - \frac{F(d_j)}{d_j^3} \right] \right\}^2}. \tag{A3}$$

In the case of a power law interaction of exponent α (26), this can be expressed in terms of Riemann's ζ function $\zeta(s)$:

$$\sum_{n=1}^{\infty} \frac{1}{n^s} \equiv \zeta(s), \quad \sum_{n=1}^{\infty} \frac{1}{(2n)^s} \equiv \frac{1}{2^s} \zeta(s), \quad \sum_{n=1}^{\infty} \frac{1}{(2n-1)^s} \equiv \left(1 - \frac{1}{2^s} \right) \zeta(s). \tag{A4}$$

The natural unit for $S(h)$ is U_0/d^2, which will be used henceforward. Therefore

$$S_0(\alpha) = -\alpha(\alpha+1)\zeta(\alpha) + \frac{\alpha(\alpha+2)\left(1 - \frac{1}{2^{\alpha+2}}\right)^2 \zeta(\alpha+2)^2}{\left(1 - \frac{1}{2^{\alpha+4}}\right)\zeta(\alpha+4)}, \tag{A5}$$

$$S_2(\alpha) = 2\alpha(\alpha+2)\left(1 - \frac{1}{2^{\alpha+2}}\right)^2 \zeta(\alpha+2)^2 \left[\frac{(\alpha+4)\left(1 - \frac{1}{2^{\alpha+6}}\right)\zeta(\alpha+6)}{\left(1 - \frac{1}{2^{\alpha+4}}\right)^2 \zeta(\alpha+4)^2} - \frac{(\alpha+5)}{\left(1 - \frac{1}{2^{\alpha+2}}\right)\zeta(\alpha+2)} \right]. \tag{A6}$$

A numerical estimate shows that $S_2(\alpha) < 0$ for all values of α, while $S_0(\alpha) \leqslant 0$ for $\alpha \leqslant 2.645$ [see Fig. 11(a)].

In the case of the 3D Coulomb potential ($\alpha = 1$) all frequencies are real and there is no instability, in agreement with Ref. [17]. On the contrary, the 3D dipolar interaction ($\alpha = 3$) leads to an instability of the regular zigzag pattern.

APPENDIX B: FINITE RANGE POTENTIALS

In this Appendix, we use the small h expansion of $S(h)$ in terms of S_0 and S_2, Eqs. (A2) and (A3), but this time for modified Bessel and Yukawa interactions. In this case we are looking for the critical interaction range where an unstable mode appears in infinite systems. We note the inverse of the dimensionless interaction range $\xi = d/\lambda_0$.

As before, the numerical estimation of $S_2(\xi)$ is negative for all ξ, and we focus on the expressions of $S_0(\xi)$. For the modified Bessel $K_0(\cdot)$ potential,

$$S_0(\xi) = \frac{\left(\sum_{p=1}^{\infty} \left\{ 2\frac{K_1[(2p-1)\xi]}{(2p-1)\xi} + K_0[(2p-1)\xi] \right\} \right)^2}{\sum_{p=1}^{\infty} \left\{ 2\frac{K_1[(2p-1)\xi]}{(2p-1)^3\xi} + \frac{K_0[(2p-1)\xi]}{(2p-1)^2} \right\}} - \sum_{p=1}^{\infty} \left[\frac{pK_1(p\xi)}{\xi} + p^2 K_0(p\xi) \right], \tag{B1}$$

where $K_1(\cdot)$ is the modified Bessel function of order 1. For the Yukawa potential,

$$S_0(\xi) = \frac{\left\{ \sum_{p=1}^{\infty} \frac{e^{-(2p-1)\xi}}{(2p-1)^3}[\xi^2(2p-1)^2 + 3\xi(2p-1) + 3] \right\}^2}{\sum_{p=1}^{\infty} \frac{e^{-(2p-1)\xi}}{(2p-1)^5}[\xi^2(2p-1)^2 + 3\xi(2p-1) + 3]} - \sum_{p=1}^{\infty} \frac{e^{-p\xi}}{p}(p^2\xi^2 + 2p\xi + 2). \tag{B2}$$

Figures 11(b) and 11(c) show the numerical estimates of expressions (B1) and (B2). They provide the critical interaction ranges resulting in unstable infinite zigzag configurations, $d/\lambda_0 > 2.04$ for modified Bessel potential and $d/\lambda_0 > 1.49$ for Yukawa potential.

[1] A. Hodgkin and R. Keynes, The potassium permeability of a giant nerve fibre, J. Physiol. **128**, 61 (1955).

[2] J. P. Schiffer, Phase transitions in anisotropically confined ionic crystals, Phys. Rev. Lett. **70**, 818 (1993).

[3] S. Seidelin, J. Chiaverini, R. Reichle, J. J. Bollinger, D. Leibfried, J. Britton, J. H. Wesenberg, R. B. Blakestad, R. J. Epstein, D. B. Hume, W. M. Itano, J. D. Jost, C. Langer, R. Ozeri, N. Shiga, and D. J. Wineland, Microfabricated surface-electrode ion trap for scalable quantum information processing, Phys. Rev. Lett. **96**, 253003 (2006).

[4] G. De Chiara, A. del Campo, G. Morigi, M. Plenio, and A. Retzker, Spontaneous nucleation of structural defects in inhomogeneous ion chains, New J. Phys. **12**, 115003 (2010).

[5] M. Mielenz, J. Brox, S. Kahra, G. Leschhorn, M. Albert, T. Schaetz, H. Landa, and B. Reznik, Trapping of topological-structural defects in coulomb crystals, Phys. Rev. Lett. **110**, 133004 (2013).

[6] B. Liu and J. Goree, Phonons in a one-dimensional yukawa chain: Dusty plasma experiment and model, Phys. Rev. E **71**, 046410 (2005).

[7] A. Melzer, Zigzag transition of finite dust clusters, Phys. Rev. E **73**, 056404 (2006).

[8] T. E. Sheridan and K. D. Wells, Dimensional phase transition in small yukawa clusters, Phys. Rev. E **81**, 016404 (2010).

[9] T. E. Sheridan and A. Magyar, Power law behavior for the zigzag transition in a yukawa cluster, Phys. Plasmas **17**, 113703 (2010).

[10] C. Coste, J.-B. Delfau, C. Even, and M. Saint Jean, Single file diffusion of macroscopic charged particles, Phys. Rev. E **81**, 051201 (2010).

[11] J.-B. Delfau, C. Coste, and M. Saint Jean, Single file diffusion of particles with long-ranged interactions: Damping and finite size effects, Phys. Rev. E **84**, 011101 (2011).

[12] J.-B. Delfau, C. Coste, and M. Saint Jean, Transverse single-file-diffusion near the zigzag transition, Phys. Rev. E **87**, 032163 (2013).

[13] T. Sheridan, Dusty plasma ring model, Phys. Scr. **80**, 065502 (2009).

[14] J.-B. Delfau, Diffusion et corrélations de particules confinées en interaction à longue portée (in French), Ph.D. thesis, Université Paris Diderot, 2013.

[15] J.-B. Delfau, C. Coste, and M. Saint Jean, Noisy zigzag transition, fluctuations, and thermal bifurcation threshold, Phys. Rev. E **87**, 062135 (2013).

[16] T. Dessup, C. Coste, and M. Saint Jean, Subcriticallity of the zigzag transition: A nonlinear bifurcation analysis (unpublished).

[17] S. Fishman, G. De Chiara, T. Calarco, and G. Morigi, Structural phase transitions in low-dimensional ion crystals, Phys. Rev. B **77**, 064111 (2008).

[18] J. E. Galvan-Moya and F. M. Peeters, Ginzburg-landau theory of the zigzag transition in quasi-one-dimensional classical wigner crystals, Phys. Rev. B **84**, 134106 (2011).

[19] E. Shimshoni, G. Morigi, and S. Fishman, Quantum zigzag transition in ion chains, Phys. Rev. Lett. **106**, 010401 (2011).

[20] G. Astrakharchik, G. De Chiara, G. Morigi, and J. Boronat, Thermal and quantum fluctuations in chains of ultracold polar molecules, J. Phys. B **42**, 154026 (2009).

[21] A. V. Straube, R. P. A. Dullens, L. Schimansky-Geier, and A. A. Louis, Zigzag transitions and nonequilibrium pattern formation in colloidal chains, J. Chem. Phys. **139**, 134908 (2013).

[22] C. Coste, J.-B. Delfau, and M. Saint Jean, Longitudinal and transverse single file diffusion in quasi-1d systems, Biophys. Rev. Lett. **09**, 333 (2014).